Applied Catalysis B: Environmental 168-169 (2015) 497–508

Contents lists available at ScienceDirect

Applied Catalysis B: Environmental

journal homepage: www.elsevier.com/locate/apcatb

Hydrogen by steam reforming of ethanol over Co–Mg incorporated novel mesoporous alumina catalysts in tubular and microwave reactors

Seval Gündüz, Timur Dogu*

Department of Chemical Engineering, Middle East Technical University, 06800 Ankara Turkey

ARTICLE INFO

Article history:
Received 21 October 2014
Received in revised form 5 January 2015
Accepted 9 January 2015
Available online 12 January 2015

Keywords:
Hydrogen
Mesoporous alumina
Cobalt
Microwave reforming

ABSTRACT

Bio-ethanol is an excellent hydrogen carrier with a good potential to be used as a resource for on-board hydrogen production. In this work, a set of new Co incorporated mesoporous alumina (MA) catalysts, which were modified with Mg, were synthesized and tested in steam reforming of ethanol. Results proved that, the synthesis route of these materials had a highly significant effect on their catalytic performances. Co@Mg–MA and Co–Mg–MA catalysts, which were prepared by direct addition of Mg into the mesoporous alumina framework, gave the best performance in steam reforming of ethanol, with very high hydrogen yield values. This was concluded to be due to the presence of Co^0 and CoO phases within the structures of these catalysts. However, Co–Mg@MA and Co@MA catalysts, which were prepared by the impregnation of Co/Mg or Co into mesoporous alumina, mainly catalyzed ethanol dehydration reaction to yield ethylene, rather than steam reforming. This was concluded to be due to the high Lewis acidity of these catalysts and the presence of cobalt aluminate phase in their structure. Activity tests of the synthesized catalysts were made both in a tubular reactor which was conductively heated and also in a focused-microwave system. Better energy utilization and more stable performance with much less coke formation were achieved in the focused-microwave reactor than the conventionally heated system.

1. Introduction

Fast depletion of fossil fuels and related environmental concerns has created growing interest for the production of chemicals and alternative fuels from renewable resources [1,2]. Hydrogen, with its very high gravimetric energy density and clean burning properties, has been considered as one of the most promising energy carriers of the future [3]. Although it is considered as the most promising fuel for fuel cells, storage, and distribution problems limit its widespread use as a transportation fuel. Since hydrogen is present in bound form in nature, economical and pollution free production of it is a very important factor from the point of view of hydrogen economy [4,5]. On-board production of hydrogen in fuel cell derived cars has been considered as a promising alternate to hydrogen storage.

Alcohols have been considered as very good candidates for on-board hydrogen production [6]. Due to its production possibilities from variety of renewable feedstock, as well as its CO_2 neutrality and low toxicity, ethanol has been considered as an excellent bio-resource for hydrogen production [3,6,7]. Main reactions taking place during steam reforming of ethanol (SRE) are the reforming reaction (R.1) and water–gas shift reaction (WGSR) (R.2).

$$C_2H_5OH + H_2O \leftrightarrow 2CO + 4H_2 \quad (R.1)$$

$$CO + H_2O \leftrightarrow CO_2 + H_2 \quad (R.2)$$

In the absence of other side reactions, six moles of H_2 could in principle be produced per mole of ethanol (R.3). However, thermodynamic limitations and the occurrence of side reactions, such as ethanol dehydrogenation, cracking, and dehydration, limit the approach to this maximum hydrogen yield value.

$$C_2H_5OH + 3H_2O \leftrightarrow 2CO_2 + 6H_2 \quad (R.3)$$

Boudouard reaction may also cause coke formation in this system. Due to the exothermic nature of this reaction, it becomes more important at low temperatures (R.4).

$$2CO \leftrightarrow CO_2 + C \quad (R.4)$$

Effectiveness of SRE for hydrogen production strongly depends upon the development of new catalysts with high activity, high

* Corresponding author. Tel.: +90 312 210 2631; fax: +90 312 210 2600.
E-mail addresses: gseval@metu.edu.tr (S. Gündüz), tdogu@metu.edu.tr (T. Dogu).

http://dx.doi.org/10.1016/j.apcatb.2015.01.006
0926-3373/

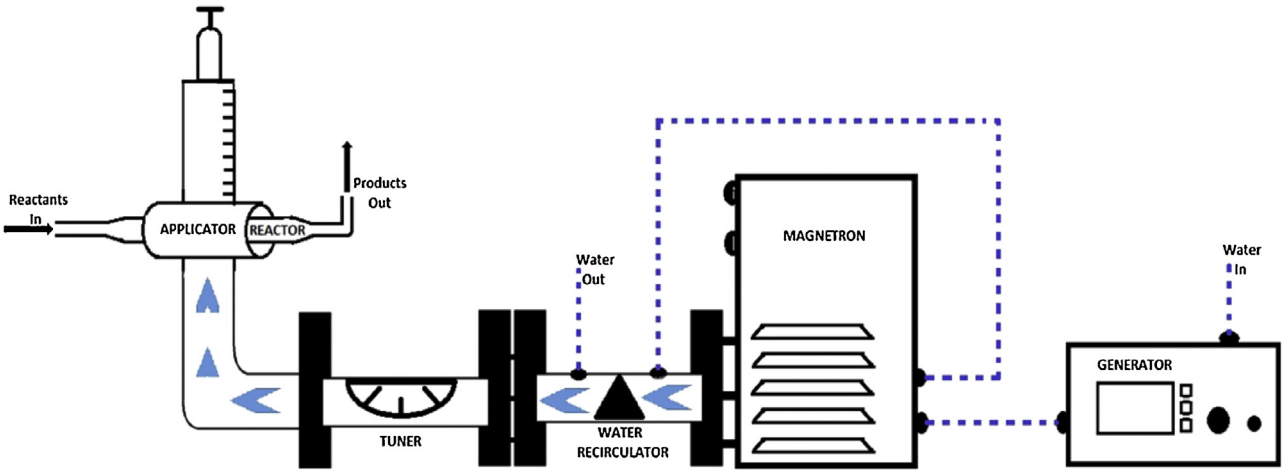

Fig. 1. Schematic diagram of reaction system with a focused-microwave heating unit.

H_2 selectivity, high stability, low diffusional resistance, low coke formation, and low cost. Due to the high cost of noble metals, recent studies were focused to Co and Ni based reforming catalysts [3,4,8–11]. Catalyst deactivation due to coke formation is one of the most important problems to be resolved for Ni based catalysts. As it was reported by Fatsikostas et al., the type of support material of Ni based materials had a strong influence on their catalytic performances and stabilities, in steam reforming of ethanol [12]. Results reported in that work also showed that, coke minimization could be achieved by use of La_2O_3 as the support material, due to

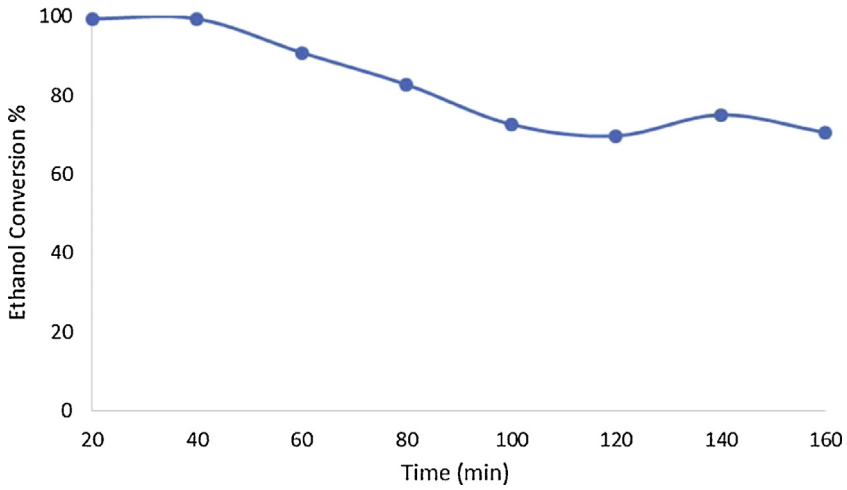

Fig. 2. Ethanol fractional conversion over Co–Mg–MA at 450 °C.

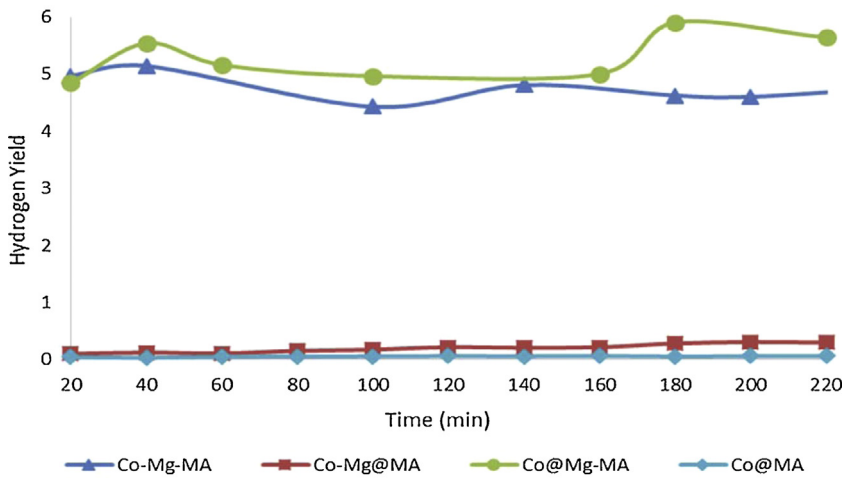

Fig. 3. Hydrogen yield values with respect to reaction time (550 °C, H_2O/EtOH = 3.2).

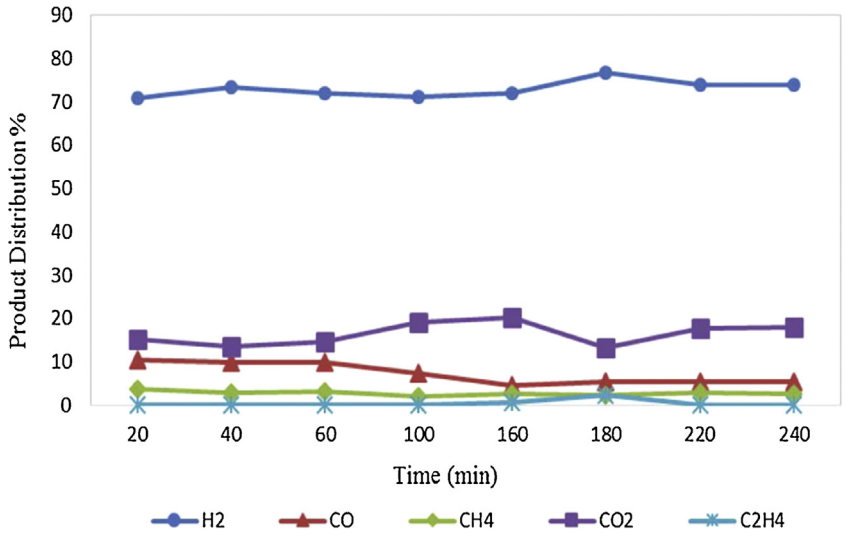

Fig. 4. Product distributions (Ar and water free percentages of all components in the gaseous product stream) observed with Co@Mg–MA at a H_2O/EtOH ratio of 3.2 at 550 °C.

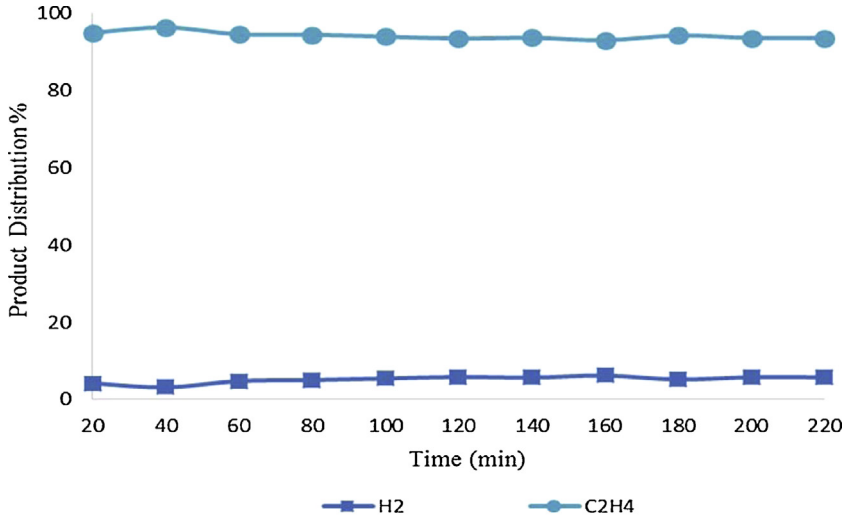

Fig. 5. Product distributions (Ar and water free percentages of all components in the gaseous product stream) observed with Co@MA.

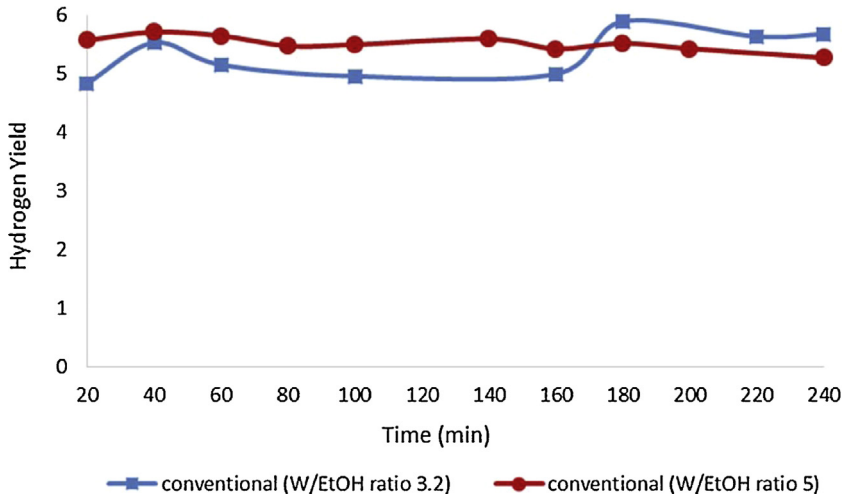

Fig. 6. Comparison of hydrogen yield values obtained at H_2O/EtOH ratios of 3.2 and 5.0 in the conventionally heated reactor (at 550 °C over Co@Mg–MA).

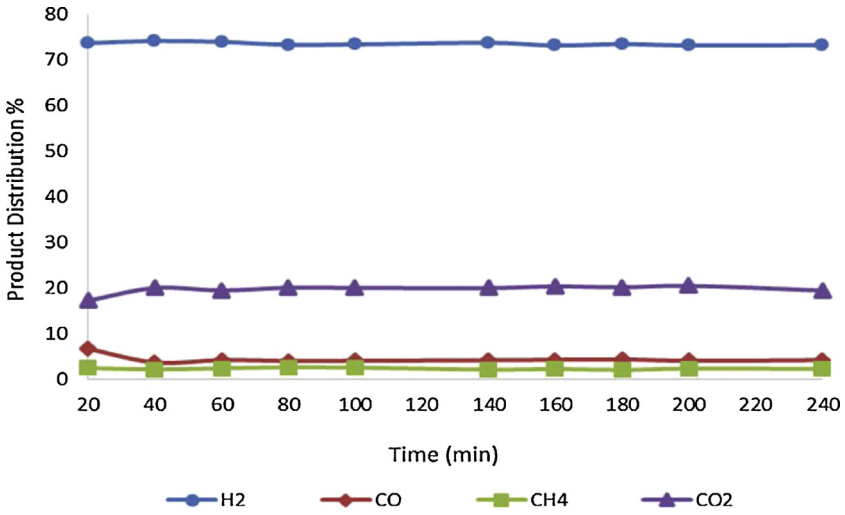

Fig. 7. Product distributions (Ar and water free percentages of all components in the gaseous product stream) observed with Co@Mg–MA at a H_2O/EtOH ratio of 5.0 at 550 °C.

formation of lanthanum oxycarbonate species on top of the Ni particles, under reaction conditions.

As far as Co based catalysts were concerned, alumina supported Co was reported to show the best catalytic performance in SRE reaction, as compared to silica, zirconia, magnesia, and carbon supported catalysts [9]. Recent advances in the synthesis of high surface area mesoporous materials with ordered pore structures opened new pathways in catalysis research [13,14]. These materials were reported to have much less transport resistances and less coke formation than the conventional microporous materials [4,15]. Mesoporous silicate structured materials, like MCM-41 and SBA-15, were tested as the catalyst supports in number of catalytic reactions [15]. However, hydrothermal stability of these materials is not very high. Hydrothermal stability of mesoporous alumina is much higher than the mesoporous silicate structured materials, even at temperatures as high as 1000 °C.

Due to the highly endothermic nature of SRE reaction, high temperatures are needed to achieve high hydrogen yield. In order to make this process economically feasible, high temperatures should be achieved with low energy input. The application of microwave energy has recently been proposed as a potential way to enhance chemical reactions [16–18]. Compared to the conventional heating processes, direct conversion of electromagnetic energy into heat can be achieved through focused microwave heating. Another advantage of microwave heating is to achieve uniform temperature distribution within the catalyst bed. However, in order to absorb microwave energy, the catalyst should be a dielectric material and it should act not only as a catalyst, but also as a microwave receptor [19].

In this paper, we presented results of SRE reaction performed both in conductively heated and microwave heated reactors using a set of new Co–Mg incorporated mesoporous alumina catalysts, which were synthesized by one-pot and impregnation routes. Significance of the catalyst synthesis route on the product distribution and the positive effect of microwave heating on reactor performance was shown.

2. Experimental and procedures

2.1. Catalyst preparation

A set of cobalt incorporated mesoporous alumina (MA) catalysts, which were modified with Mg, were synthesized by two different routes, namely direct synthesis and impregnation. Mesoporous

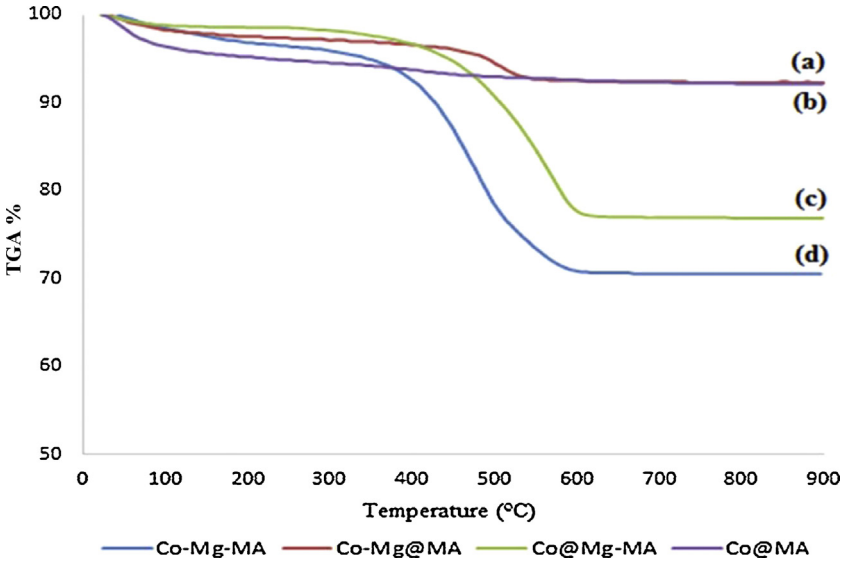

Fig. 8. TGA analysis of used catalysts (a) Co–Mg@MA, (b) Co@MA, (c) Co@Mg–MA, and (d) Co–Mg–MA.

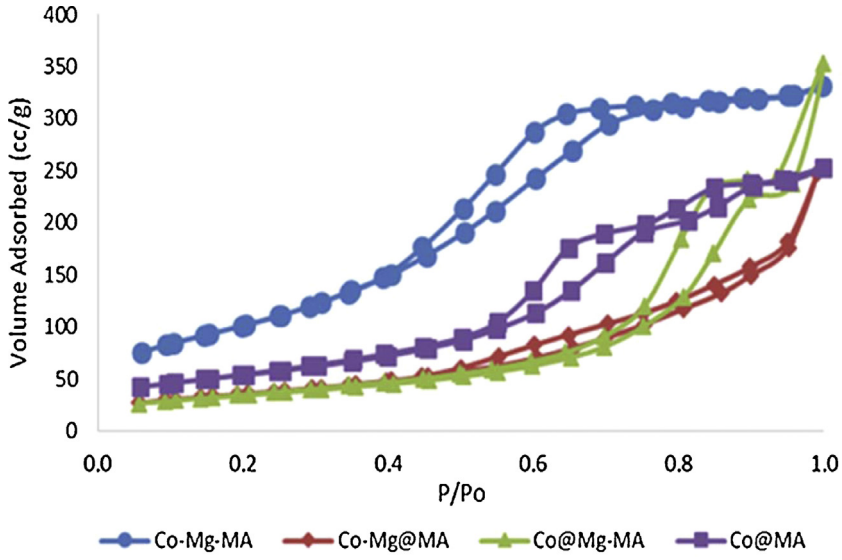

Fig. 9. Nitrogen physisorption isotherms of materials.

alumina (MA) type support material was synthesized following the 'evaporation-induced-self-assembly' (EISA) method [14]. For MA synthesis, $(EO)_{20}(PO)_{70}(EO)_{20}$ triblock copolymer (Pluronic P123) was used as the surfactant. It was dissolved in anhydrous ethanol and then gradually mixed with a solution of aluminum isopropoxide. Solvent evaporation was performed at 60 °C and the resulting product was calcined at 700 °C for 6 h, in the presence of air flow. After synthesis of the support material (MA), Co or Co–Mg was impregnated into it, in order to obtain catalysts having Co/Al and Mg/Al ratios of 0.1 and 0.25, respectively. Cobalt acetyl acetonate and $MgCl_2{\cdot}6H_2O$ were used as the Co and Mg sources, respectively. Finally, the solid product was calcined at 700 °C. Synthesized catalysts were reduced with hydrogen gas at 650 °C for 4 h just before each experiment. Resulting Co and Co–Mg containing mesoporous alumina catalysts were named as Co@MA and Co–Mg@MA, respectively.

In the case of direct synthesis method, Co acetyl acetonate and $MgCl_2{\cdot}6H_2O$ were separately dissolved in deionized water, and added drop-wise to the solution of aluminum isopropoxide and Pluronic 123. Co/Al and Mg/Al ratios were adjusted as the same as in the case of impregnation route. Produced solid material was calcined and reduced at the same conditions as in the case of impregnation. This catalyst was named as Co–Mg–MA.

In order to investigate the effect of Mg incorporation procedure on the catalytic performance of the synthesized materials, a fourth catalyst was synthesized following direct addition of Mg into the MA structure (Mg–MA) and impregnation of Co into this Mg–MA type support material. This catalyst was named as Co@Mg–MA. Co/Al and Mg/Al ratios were again adjusted as 0.1 and 0.25, respectively, during the synthesis of this material.

2.2. Characterization

Textural properties of the synthesized materials were examined by nitrogen adsorption–desorption measurements, using a Quantachrome Autosorb-6 instrument. Crystal structures were determined by XRD analysis, using a Rigaku Ultima IV XRD instrument. XPS (PHI 5000 Versa Probe with a monochromatized Al Kα X-ray source) and TEM (Jem Jeol 2100F 200 kV HRTEM) instruments were also used for the characterization of the synthesized

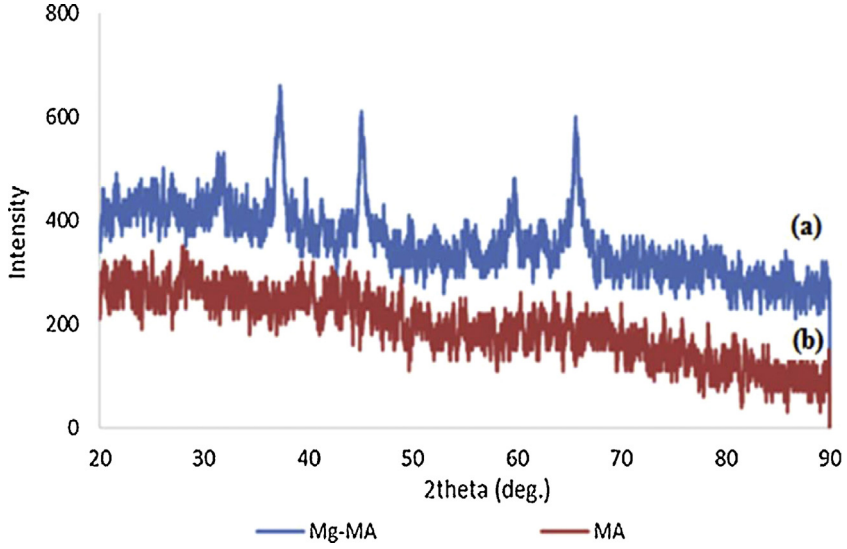

Fig. 10. XRD patterns of (a) Mg–MA and (b) MA.

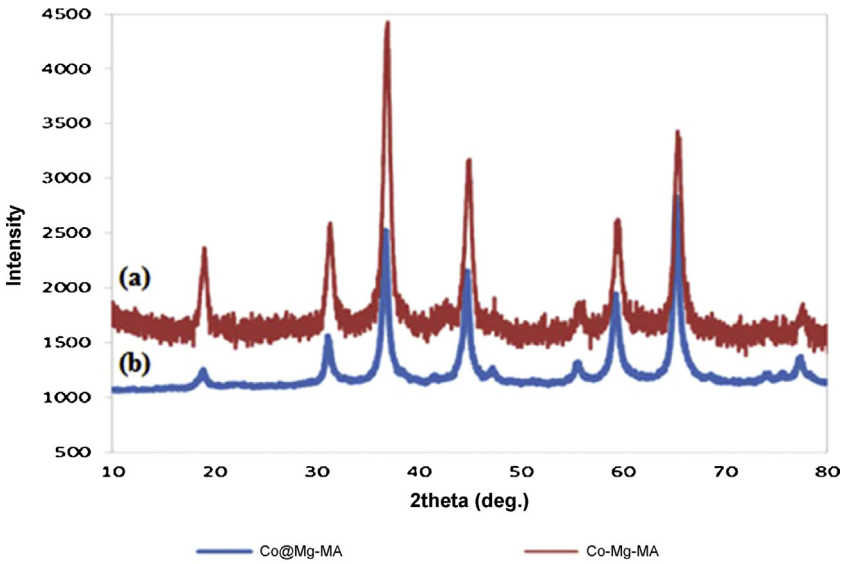

Fig. 11. XRD patterns of (a) Co–Mg–MA and (b) Co@Mg–MA.

catalysts. Collected XPS data were corrected for charge shifting, using standard C 1s binding energy of 284.5 eV and curve fitting was performed with XPS-peak v4.1 software package. Since the materials were inorganic, Shirley-type background fitting was used to determine spectra baselines and deconvolution was done using 80% Lorentzian-20% Gaussian combination peaks. Diffuse reflectance FTIR spectra (DRIFTS) of pyridine adsorbed samples were also obtained by use of a PerkinElmer Spectrum One instrument. Such data gave information about the acidity of the synthesized materials. Thermal analysis (TGA–DTA) of the used catalysts was performed by use of a Shimadzu Model TA-60 WS instrument, to determine the amount of coke formed on the catalyst during reaction.

2.3. Convectively heated reaction system

Catalytic tests for SRE over the synthesized catalysts were conducted in a fixed bed quartz tubular reactor (1.3 cm in diameter), which was placed into a tubular furnace. Catalyst (1.5 g) was placed at the center of the reactor tube and supported by quartz wool from both ends. Liquid feed stream, with a H_2O/EtOH molar ratio of 3.2, was introduced into an evaporator, by use of a liquid injection pump. WHSV of these activity tests was 4.8 h^{-1}. Some experiments were repeated with a higher H_2O/EtOH ratio of 5.0. This stream was mixed with Ar in the evaporator (20 mL/min H_2O + EtOH vapor, 30 mL/min Ar) and then introduced into the reactor. A condenser was placed between the reactor and gas chromatograph (GC) to collect water and other liquefied components (if any). On-line chemical analysis of the gaseous product stream was achieved by using a gas chromatograph (Agilent Technologies 6850). Composition of the condensed stream was also periodically analyzed.

2.4. Focused-microwave reactor system

A set of experiments were also performed in a reactor which was heated by a focused microwave source. A schematic diagram of the reaction system installed with the focused-microwave heating unit is shown in Fig. 1. Selection and design of the components of microwave reactor were performed with the contribution of SAIREM Co. Temperature measurement of the catalyst bed is achieved by use of an infrared pyrometer, which is placed at a location looking directly to the catalyst bed from a distance of 2 cm.

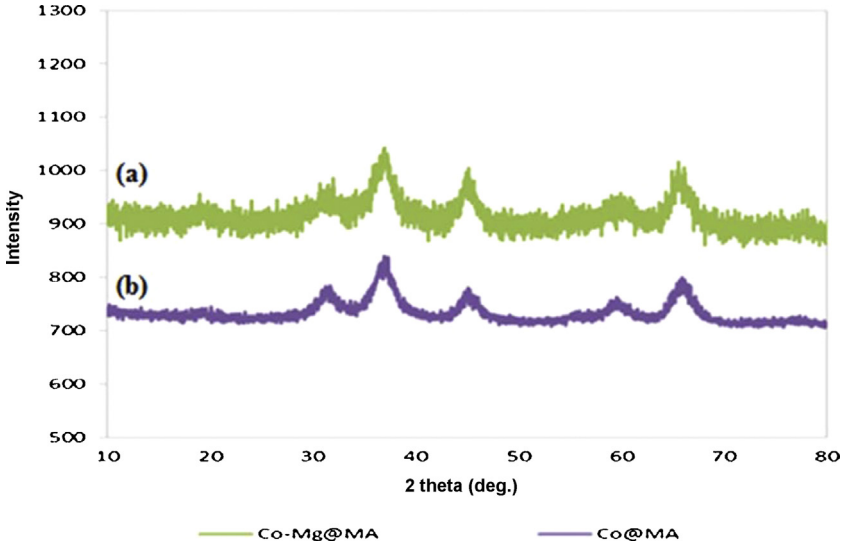

Fig. 12. XRD patterns of (a) Co–Mg@MA and (b) Co@MA.

3. Results and discussion

3.1. Tubular reactor SRE results

Synthesized catalysts were tested in steam reforming of ethanol (SRE) reaction in the fixed-bed flow reactor, mostly at 550 °C and atmospheric pressure. Some initial experiments were performed at a lower temperature of 450 °C. Catalytic activities of these materials were evaluated according to ethanol conversion, hydrogen yield, and product distributions. Hydrogen yield values were calculated by dividing moles of hydrogen produced by the moles of ethanol fed to the reactor.

Initial experiments performed at 450 °C indicated catalyst activity decrease as a function of reaction time, which was mainly caused by coke formation through Boudouard reaction (R.4). A typical result obtained with Co–Mg–MA is shown in Fig. 2. As shown in this figure, ethanol conversion decreased from complete conversion to about 70%, within a reaction period of 4 h at 450 °C. However, highly stable catalytic performance was observed at higher temperatures. Hence, most of the experiments were performed at 550 °C. Complete conversion of ethanol was achieved at 550 °C, at a space time of less than a second, with all of the new catalysts synthesized in this work. Analysis of vapor stream leaving the reactor and the condensed liquid did not contain any ethanol in these experiments. This result indicated that, the catalysts synthesized in this work were very active for SRE. However, a drastic difference was observed in the hydrogen yield values obtained with the materials prepared by impregnating Co or Co–Mg into MA (Co@MA and Co–Mg@MA) and the materials prepared by the one-pot route for the incorporation of Mg into MA (Co@Mg–MA and Co–Mg–MA) (Fig. 3). Co–Mg–MA and Co@Mg–MA gave very high H_2 yield values, while the H_2 yield values obtained with Co@MA and Co–Mg@MA were close to zero. Co@Mg–MA gave the highest hydrogen yield value of about 5.2 per one mole of ethanol fed to the reactor.

Differences of the catalytic performances of these four catalysts are more clearly seen in the product distributions. Time variation of product stream compositions observed with the Co@Mg–MA and Co@MA catalysts are shown in Figs. 4 and 5, respectively. As illustrated in Fig. 4, the main product was hydrogen over Co@Mg–MA catalyst. Hydrogen mole fraction obtained in the product stream over this catalyst was about 0.71 during the first 100 min of the reaction. CO and CO_2 were the main carbon containing products and their mole fractions were about 0.09–0.10 and 0.18, respectively, within the same period. If we consider the occurrence of SRE (R.1) and WGS (R.2) reactions only, a CO_2 mole fraction of 0.18 would correspond to a CO mole fraction of 0.094, for complete conversion of ethanol. This value agreed quite well with the experimental value of CO mole fraction in the product stream. Corresponding hydrogen mole fraction was calculated as about 0.73 from the stoichiometry of reactions (R.1) and (R.2). This value was slightly higher than the experimental H_2 mole fraction of 0.71. This difference was considered to be mainly due to the formation of small amount of methane (~3% in the product stream), through ethanol decomposition and/or reverse dry reforming reaction (RDR) (R.5). Formation of some CH_4 through RDR reaction is thermodynamically favored at the reaction temperature. Decrease of CO mole fraction, with an increase of CO_2 mole fraction in the product stream, at reaction times higher than 100 min (Fig. 4), indicated facilitation of coke formation through Boudouard reaction (R.4).

$$2CO + 2H_2 \leftrightarrow CO_2 + CH_4 \quad (R.5)$$

As it will be discussed in the catalyst characterization section of this paper, XRD and XPS analysis proved the presence of Co^0 and CoO clusters in these materials. As it was also reported in the literature, these forms of cobalt were highly active in SRE [3,23–27]. During the reduction process of the catalyst, first Co_3O_4 was expected to reduce to CoO in the temperature range of 473–673 K [23,24]. Reduction of CoO to more active Co^0 was reported to take place at much higher temperatures, giving broad TPR peaks. Apparently, reduction process of cobalt oxide to Co^0 is strongly influenced by the interaction with the support material. An equilibrium state between CoO and Co^0 was reported [3,28] during steam reforming of ethanol. As reported by Hyman and Vohs [26], both Co^0 and CoO were quite active for ethanol dehydrogenation. However, C—C bond cleavage was shown to be mainly due to the presence of Co^0 [25,27].

In the cases of Co@MA and Co–Mg@MA catalysts, the main product was ethylene (Fig. 5). Formation of significant amount of ethylene indicated that the main reaction was ethanol dehydration, rather than SRE. This result implied that Co–Mg@MA and Co@MA catalysts should be more acidic, which would favor ethanol dehydration to ethylene. As it will also be discussed later in this paper, DRIFTS analysis of pyridine adsorbed materials, proved much higher Lewis acidity of these materials as compared to Co@Mg–MA and Co–Mg–MA. Apparently, incorporation of Mg into the framework of MA during the one-pot synthesis route caused decrease of the acidity of MA. However, impregnation of Mg into MA did not significantly affect the acidity of the final product. Also, XRD–XPS analysis of the synthesized catalysts proved the presence of cobalt aluminate phase in Co–Mg@MA and Co@MA (Section 3.2). Cobalt aluminate is known as a highly stable compound and reduction of this compound is quite difficult. The absence of Co^0 and CoO in Co–Mg@MA and Co@MA caused inactivity of these materials towards SRE.

In order to test the effect of H_2O/EtOH ratio on product distributions, another experiment was performed with a H_2O/EtOH ratio of 5.0 at 550 °C, over the catalyst giving the highest hydrogen yield (Co@Mg–MA). Comparison of hydrogen yield values obtained over this catalyst with H_2O/EtOH ratios of 3.2 and 5.0, is given in Fig. 6. Increase of H_2O/EtOH ratio caused more stable performance of the catalyst, with slightly higher hydrogen yield values. Product distributions given in Fig. 7 also showed highly stable product stream compositions with a H_2O/EtOH ratio of 5.0. As it was expected from the stoichiometry of water gas shift reaction, some increase of CO_2 mole fraction with a corresponding decrease in CO mole fraction was observed with an increase of steam to ethanol ratio.

In order to analyze coke formation during SRE reaction, TGA characterization of the used catalysts was performed and illustrated in Fig. 8. As shown in this figure, coke formation was negligible with the catalysts yielding ethylene as the main product. However, about 20% coke formation was observed over 0.15 g catalyst within a reaction period of 4 h, with the catalysts giving high hydrogen yields. Coke formation was considered to be mainly due to Boudouard reaction (R.4). Some contribution of ethanol decomposition to coke formation is also expected. Results of carbon balances, which were made considering the carbon in the feed and gaseous product streams, were quite satisfactory, especially in the experiments yielding low coke formation. However, if coke formation was high, amount of coke had to be included to the carbon balance. In fact, amount of coke evaluated from the TGA analysis agreed quite well with the amount of coke estimated from the difference of carbon in the feed and gaseous product streams.

3.2. Catalyst characterization

In order to understand the reasons of performance difference of the catalysts tested in this study, several characterization studies were conducted. To investigate the textural properties of the synthesized catalysts, nitrogen physisorption characterization method was applied. Surface area values, pore diameters, and pore volumes of the synthesized catalysts are shown in Table 1. Both surface area and pore volume values decreased by the impregnation of Mg

Table 1
Textural properties of synthesized materials.

Material	BET surface area (m^2/g)	BJH pore volume (cc/g)	BJH pore diameter (nm)
Co–Mg–MA	384.3	0.56	3.8
Co–Mg@MA	129.4	0.39	4.3
Co@Mg–MA	123.1	0.57	9.7
Co@MA	192.7	0.42	5.6
MA	212.0	0.51	5.1

and Co into MA, indicating blocking of some of the pores by the impregnated metals. Some decrease in the pore diameter was also observed as a result of impregnation. However, direct addition of Mg and Co into the MA structure caused some increase of both the surface area and pore volume.

Nitrogen adsorption–desorption isotherm curves of Co based catalysts are shown in Fig. 9. Well-defined and steep hysteresis loops with parallel adsorption–desorption branches are the characteristics of formation of ordered mesopores with a narrow pore size distribution. Such hysteresis loops were observed for Co–Mg–MA and Co@Mg–MA catalysts synthesized by direct addition of Mg into the MA structure. However, in the case of Co and Mg impregnated materials (Co–Mg@MA and Co@MA), this characteristic behavior was significantly lost, indicating deformations in the long-range order of mesopores.

XRD patterns of MA and Mg–MA are shown in Fig. 10. This figure clearly indicated that MA had an amorphous structure. Peaks observed in XRD pattern of Mg modified MA correspond to $MgAl_2O_4$ spinel structure [20]. In the XRD patterns of Co–Mg–MA and Co@Mg–MA (Fig. 11), eight diffraction peaks were observed at 2θ values of 19°, 31°, 37°, 44°, 55°, 59°, 65°, and 78°. For pure Co_3O_4, the ratio of intensities of [3 1 1] plane peak (at 37°) and [4 0 0] plane peak (at 44°) should be nearly 4 [21]. However, this ratio was about 2 and 1.5 in the XRD patterns of Co–Mg–MA and Co@Mg–MA, respectively. These results indicated that Co_3O_4 was not the only cobalt form in these two catalysts. The main [1 1 1] plane peak of metallic Co is also expected at a 2θ value of 44°. These results indicated the presence of metallic Co, as well as Co_3O_4 in Co–Mg–MA and Co@Mg–MA catalysts. Another small peak observed in the XRD patterns of these catalysts (Fig. 11) was at a 2theta value of 42.4, which indicated that CoO was also present in these catalysts [3]. XRD patterns of Co@MA and Co–Mg@MA indicated that these materials were less crystalline (Fig. 12).

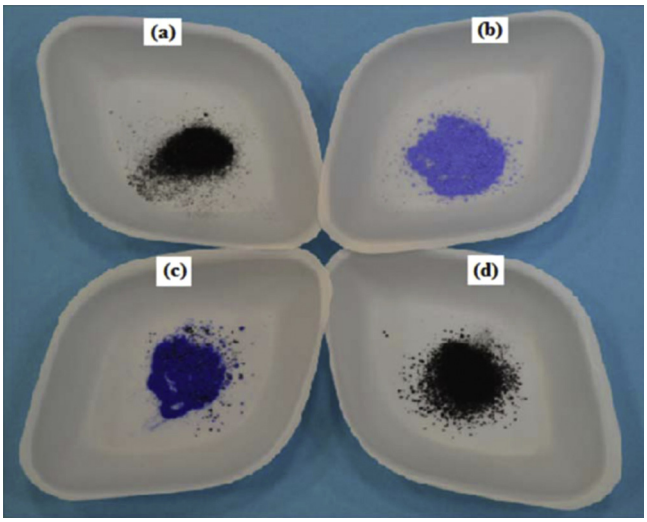

Fig. 13. Color of catalysts (a) Co–Mg–MA, (b) Co–Mg@MA, (c) Co@MA, and (d) Co@Mg–MA.

The colors of the synthesized materials also gave a clear indication of the catalyst composition (Fig. 13). The color of $CoAl_2O_4$ is well known as Thenard's blue [22]. Blue color of Co@MA and Co–Mg@MA catalysts indicated the presence of $CoAl_2O_4$ phase in these materials. However, the colors of Co_3O_4 and CoO are both black.

Fig. 14 shows the X-ray photoelectron spectra of the synthesized materials in the Co 2p region. XPS results supported the conclusions reached from XRD and color analysis. In agreement with the literature [3], curve fitting in the Co $2p_{3/2}$ region suggested the presence of three features, which were assigned to Co^0 (779 eV), Co^{2+} (781.4 eV), and a shake-up component associated with Co^{2+} species, over Co–Mg–MA and Co@Mg–MA catalysts. All these results

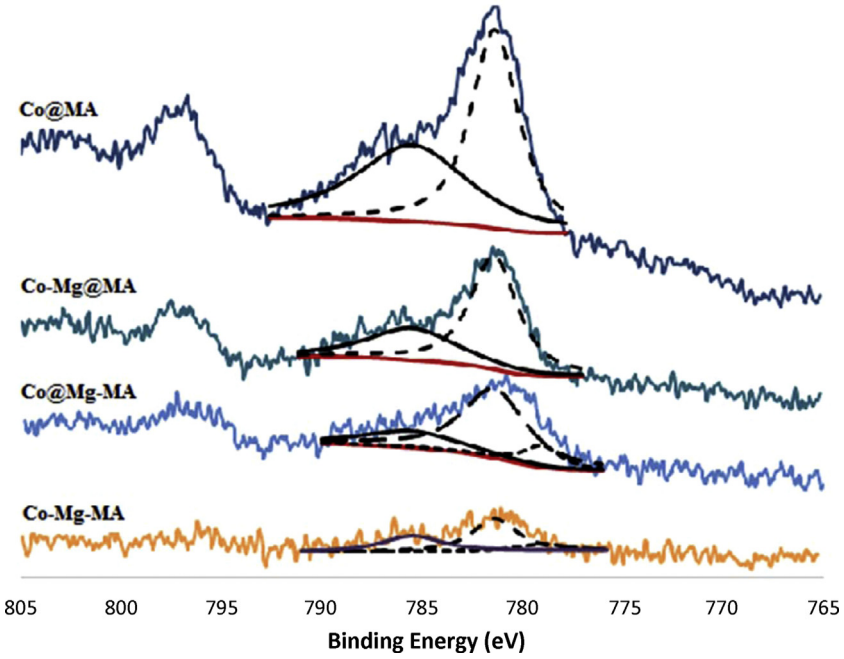

Fig. 14. X-ray photoelectron spectra of the catalysts.

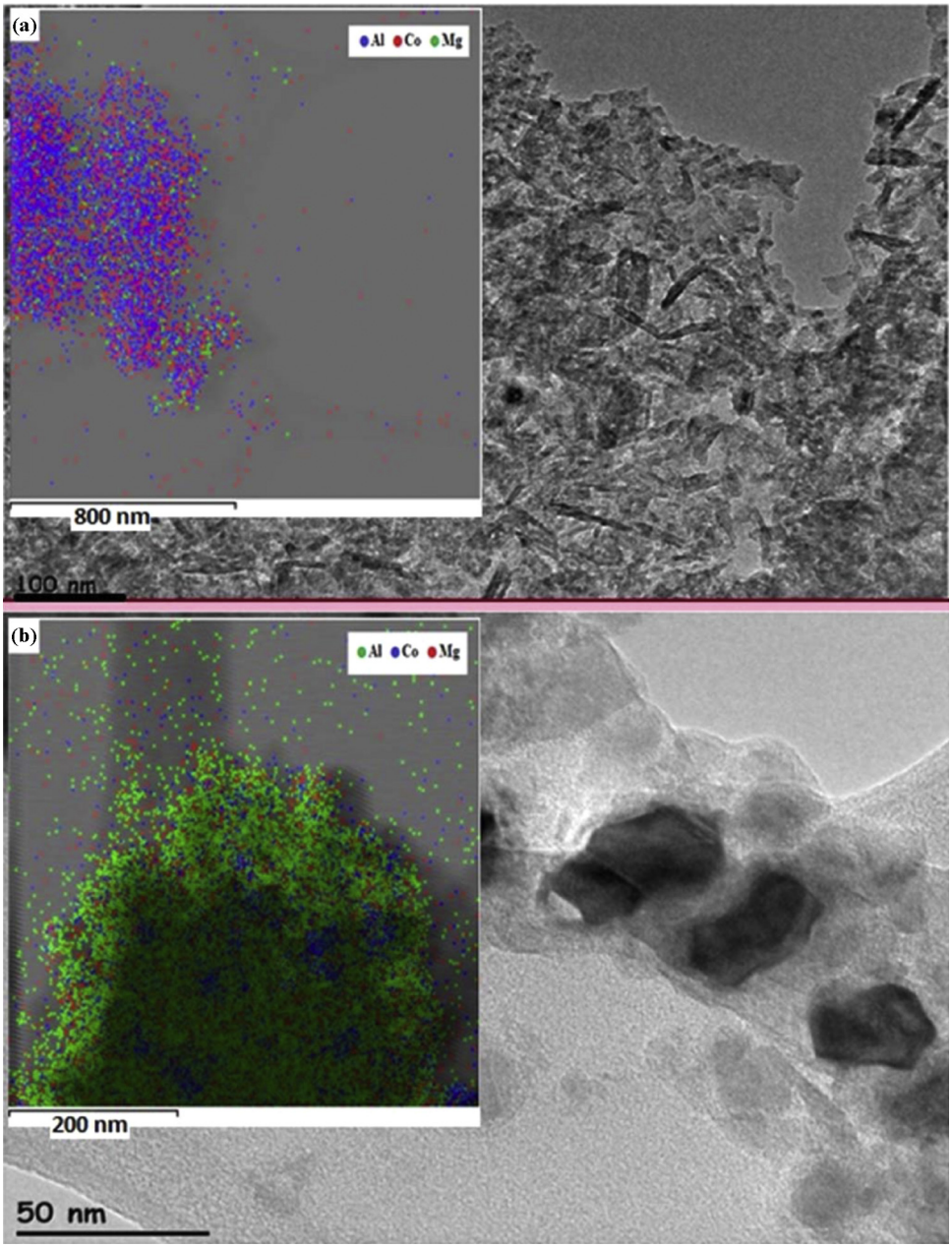

Fig. 15. TEM images and mapping of (a) Co–Mg@MA and (b) Co@Mg–MA.

indicated the presence of metallic cobalt and CoO particles on the surfaces of Co–Mg–MA and Co@Mg–MA catalysts.

Curve fitting of XPS of Co–Mg@MA and Co@MA catalysts indicated the presence of two features, which were assigned to Co^{2+} main peak and Co^{2+} shake-up component. These results showed that metallic Co was not present on the surface of Co@MA and Co–Mg@MA catalysts. In agreement with the literature [23,24], approximately 0.2 eV increase of the spin-orbital splitting peak of Co $2p_{1/2}$ (at about 797 eV) of Co–Mg@MA and Co@MA catalysts, supported the conclusion that Co^{2+} was in cobalt aluminate ($CoAl_2O_4$) form on these materials.

XRD and XPS and color analysis results of the catalysts were in agreement with the activity performance results. Due to the absence of Co^0 and CoO species in their structure, Co@MA and Co–Mg@MA were not successful catalysts for SRE reaction, with dramatically low hydrogen yield values.

TEM images of and mapping analysis of Co–Mg@MA and Co@Mg–MA catalysts indicated that direct addition of Mg into MA (Co@Mg–MA) resulted in a uniform distribution of magnesium in the catalyst framework (Fig. 15b). However, in the case of Mg impregnated catalyst (Co–Mg@MA), distribution of Mg was not uniform, but accumulated at certain locations (Fig. 15a).

Fig. 16 illustrates the DRIFT spectra of pyridine adsorbed catalysts. Transmission bands observed at 1445 and 1590 cm^{-1} correspond to the Lewis acid sites. Results indicated that, while the Lewis acid intensity of the Co–Mg@MA catalyst prepared with impregnation of Co and Mg was quite high, it was very low for the Co–Mg–MA catalyst, which was synthesized by direct addition of Co and Mg. DRIFT spectra results were also in agreement with the catalytic activity results. Co–Mg@MA and Co@MA, which have higher IR intensity values of Lewis acid sites, mainly catalyzed ethanol dehydration reaction rather than SRE. Another set of SRE

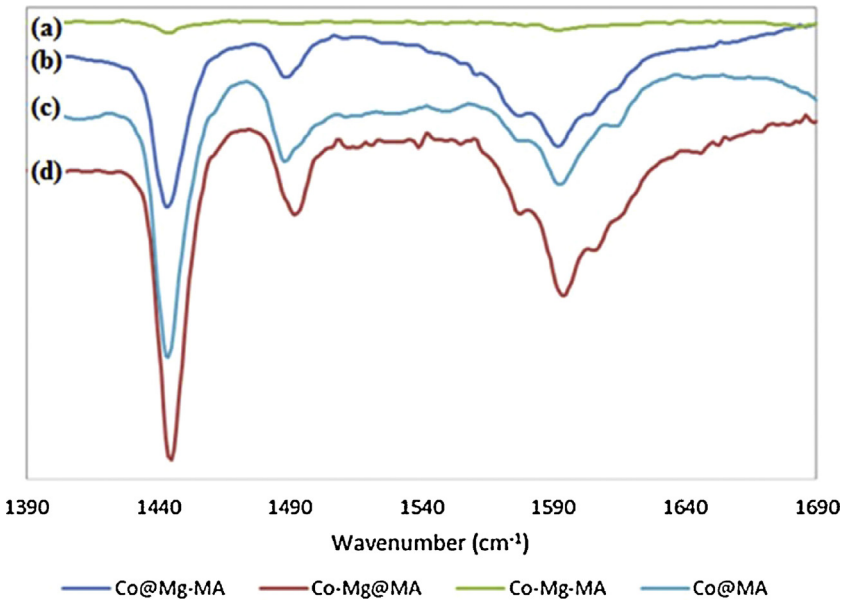

Fig. 16. DRIFT spectra of (a) Co–Mg–MA, (b) Co@Mg–MA, (c) Co@MA, and (d) Co–Mg@MA.

experiments, which were performed by the use of pure MA as the catalyst, also indicated that the main reaction product was ethylene in that system. This result indicated that, ethanol dehydration took place mainly on the acid sites of the MA support material.

3.3. Microwave reactor test results

Since the microwave absorption capacity of the synthesized catalysts was quite low, they were physically mixed with activated carbon at a ratio of 3:1 (0.15 g of catalyst and 0.05 g of activated carbon) and this mixture was charged to the reactor. Initially, generator power was set to 870 W and microwave was focused on the catalyst bed in order to create arcs to initiate microwave heating. The first moment that the arc appeared is shown in Fig. 17.

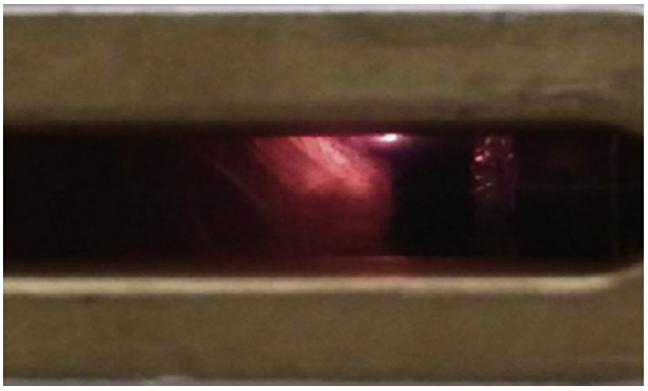

Fig. 17. Photograph of first moment of arc formation.

Within 2–3 min after the start of the experiment, catalyst bed bulk temperature increased to 560 °C, then the power was decreased and finally kept constant at 300 W, in order to keep the temperature in the range of 550–560 °C. Although 300 W microwave power was sent to the system, catalyst-activated carbon mixture absorbed only 10 W, while the rest of microwave was absorbed by cooling water in the recirculator, which was placed between the magnetron and applicator.

Hydrogen yield values obtained in the reaction systems with both conventional heating and microwave heating were compared

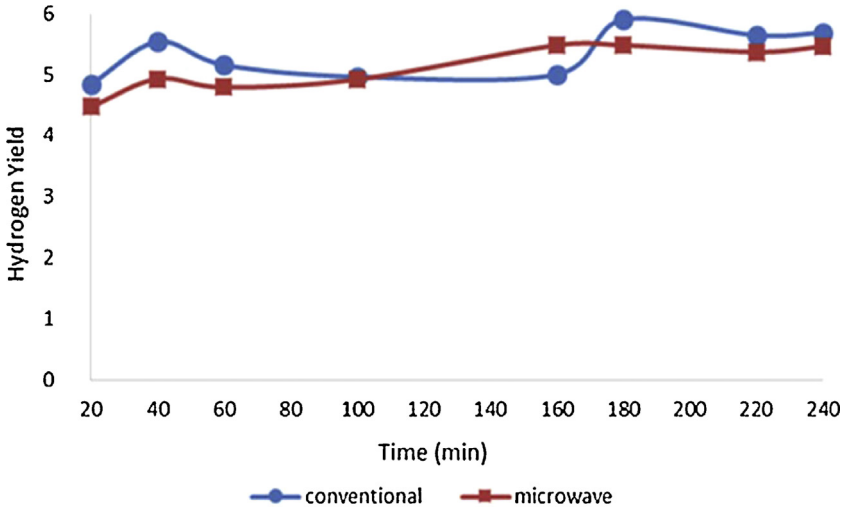

Fig. 18. H_2 yield of Co@Mg–MA, in both conventionally heated and microwave reactors.

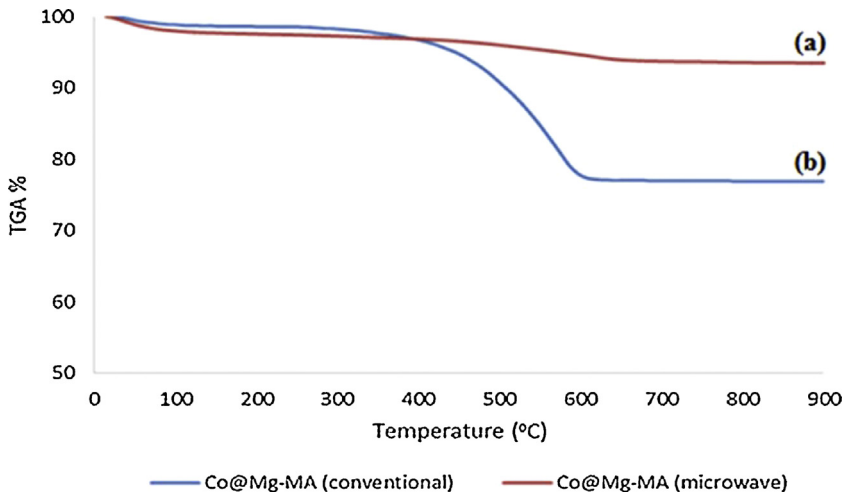

Fig. 19. TGA analysis of used Co@Mg–MA in (a) microwave and (b) conventional reactors.

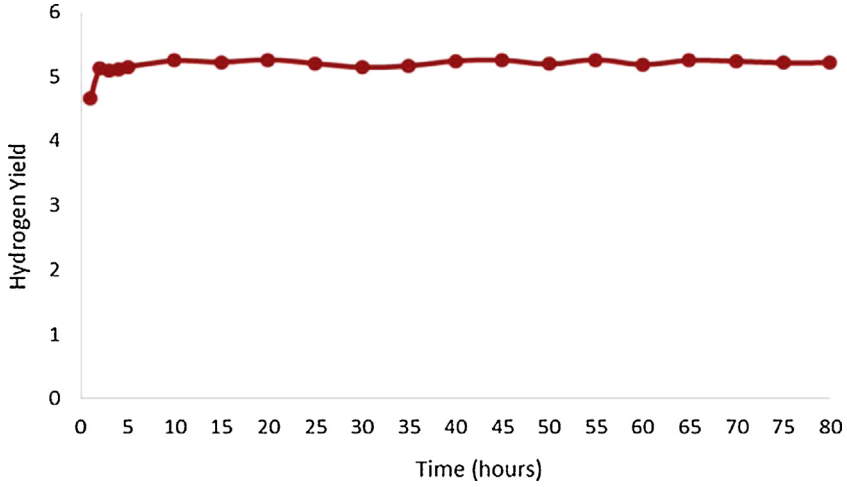

Fig. 20. H_2 yield of Co@Mg–MA in the MW reactor system (long-term stability test).

in Fig. 18. Results indicated comparable H_2 yield values. A more important result obtained in the microwave system was related to the coke formation. In the case of microwave heating, coke formation was much less than the coke formation observed in the conventionally heated system (Fig. 19). In fact, amount of coke formed in the microwave system was negligibly small during a reaction period of 5 h.

These observations could be explained by the fact that temperature gradients were lowered in the microwave reactor. In the case of conventional heating, temperature gradients within the catalyst bed are inevitable for such an endothermic reaction. Since the thermodynamics of coke formation by Boudouard reaction is more favorable at low temperatures, such temperature gradients might have caused coke formation at the low temperature locations. Product distributions obtained in the microwave and conductively heated reactors also supported this conclusion, giving more CO than CO_2 in the microwave reactor (20% CO and 6% CO_2 in product stream), while Boudouard reaction yielded more CO_2 in the conductively heated reactor (6% CO and 19% CO_2). Higher CO formation observed in the microwave reactor can be linked to the decrease of coke formation due to lack of cold spots. Decreased contribution of water gas shift reaction in the microwave reactor has also been considered as a possibility for less CO_2 formation in this system. However, in that case we would also expect to obtain lower hydrogen yield values in the microwave system than the conventionally heated reactor. Since hydrogen yield values obtained in the conventionally heated and microwave heated systems were quite comparable, contribution of this factor was considered as a quite weak possibility.

In order to investigate the catalyst stability and reliability of microwave reactor, a set of time-on stream reaction tests, extending up to 80 h, were also performed in this system. As shown in Fig. 20, hydrogen yield was highly stable over the Co@Mg–MA catalyst in the microwave reactor, during a reaction period of 80 h. This was considered to be due to lowering of coke formation in the reactor which was heated by a focused microwave source.

4. Conclusions

Effect of synthesis route on the catalytic performances of Co–Mg incorporated mesoporous alumina materials was investigated in this study. Also, the activity test results obtained in a convectively heated fixed bed flow reactor were compared with the results obtained in a reactor which was heated by a focused microwave source. Results proved advantages of the microwave system from the points of view of achieving more stable operation with much less coke formation. From the results presented in this manuscript, following conclusions can be drawn:

1. Direct addition of Mg into the MA framework resulted in the formation of highly active Co^0 and CoO clusters. Direct addition of Mg also decreased Lewis acidity of MA, eliminating ethylene formation as a result of ethanol dehydration reaction.
2. Co@Mg–MA and Co–Mg–MA catalysts prepared by direct addition of Mg into the MA framework gave the best performance in SRE reaction with very high hydrogen yield values. This was concluded to be due to the presence of Co^0 and CoO phases within their structure.
3. Co–Mg@MA and Co@MA catalysts prepared by the impregnation route contained cobalt aluminate phase and mainly catalyzed ethanol dehydration reaction to yield ethylene, due to their highly acidic nature.
4. Highly stable catalytic performance and more efficient energy utilization were obtained in the focused microwave reactor as compared to conventionally heated reactor. Temperature uniformity within the catalyst bed of the microwave reactor helped to lower coke formation by eliminating cold spots in the bed.

Acknowledgements

TUBITAK grant 111M338, METU Research Fund and the support of Turkish Academy of Sciences are gratefully acknowledged. The authors also thank the Central Laboratory of METU for the characterization results of the synthesized materials.

References

[1] C. Song, Global challenges and strategies for control conversion and utilization of CO_2 for sustainable development involving energy catalysis, adsorption and chemical processing, Catal. Today 115 (2006) 2–32.
[2] T. Dogu, D. Varisli, Alcohols as alternatives to petroleum for environmentally clean fuels and petrochemicals, Turk. J. Chem. 31 (2007) 551–567.
[3] B. Bayram, I.I. Soykal, D. Von Deak, J.T. Miller, U.S. Ozkan, Ethanol steam reforming over Co-based catalysts: investigation of cobalt coordination environment under reaction conditions, J. Catal. 284 (2011) 77–89.
[4] S. Gunduz, T. Dogu, Sorption-enhanced reforming of ethanol over Ni- and Co-incorporated MCM-41 type catalysts, Ind. Eng. Chem. Res. 51 (2012) 8796–8805.
[5] R. Shinnar, Hydrogen economy, fuel cells and electric cars, Technol. Soc. 25 (2003) 455–476.
[6] A. Haryanto, S. Fernando, N. Murali, S. Adhikari, Current status of hydrogen production techniques by steam reforming of ethanol: a review, Energy Fuels 19 (2005) 2098–2106.
[7] L.F. Brown, Comparative study of fuels for on-board hydrogen production for fuel-cell powered automobiles, Int. J. Hydrogen Energy 26 (2010) 381–397.
[8] H. Song, L. Zhang, U.S. Ozkan, Investigation of the reaction network in ethanol steam reforming over supported cobalt catalysts, Ind. Eng. Chem. Res. 49 (2010) 8984–8989.
[9] F. Haga, T. Nakajima, H. Miya, S. Mishima, Catalytic properties of supported cobalt catalysts for steam reforming of ethanol, Catal. Lett. 48 (1997) 223–227.
[10] J. Llorca, N. Homs, J. Sales, P.R. de la Piscina, Efficient production of hydrogen over supported cobalt catalysts from ethanol steam reforming, J. Catal. 209 (2002) 306–317.
[11] H. Song, L. Zhang, R.B. Watson, D. Braden, U.S. Ozkan, Investigation of bio-ethanol steam reforming over cobalt-based catalysts, Catal. Today 129 (2007) 346–354.
[12] A.N. Fatsikostas, D.I. Kondarides, X.E. Verykios, Production of hydrogen for fuel cells by reformation of biomass-derived ethanol, Catal. Today 75 (2002) 145–155.
[13] C.T. Kresge, M.E. Leonowicz, W.J. Roth, J.C. Vartuli, J.S. Beck, Ordered mesoporous molecular sieves synthesized by a liquid crystal template mechanism, Nature 359 (1992) 710–712.
[14] Q. Yuan, A. Yin, C. Luo, L. Sun, Y. Zhang, W. Duan, H. Liu, C. Yan, Facile synthesis for ordered mesoporous aluminas with high thermal stability, J. Am. Chem. Soc. 130 (2008) 3465–3472.
[15] H. Arbag, S. Yasyerli, N. Yasyerli, G. Dogu, Activity and stability enhancement of Ni–MCM-41 catalysts by Rh incorporation for hydrogen from dry reforming of methane, Int. J. Hydrogen Energy 35 (2010) 2296–2304.
[16] A. Dominguez, B. Fidalgo, Y. Fernandez, J.J. Pis, J.A. Menendez, Microwave-assisted catalytic decomposition of methane over activated carbon for CO_2-free hydrogen production, Int. J. Hydrogen Energy 32 (2007) 4792–4799.
[17] B. Fidalgo, A. Dominguez, J.J. Pis, J.A. Menendez, Microwave-assisted dry reforming of methane, Int. J. Hydrogen Energy 33 (2008) 4337–4344.
[18] X. Zhang, C.S.M. Lee, D.M.P. Mingos, D.O. Hayward, Oxidative coupling of methane using microwave dielectric heating, Appl. Catal. A: Gen. 249 (2003) 151–164.
[19] J.A. Menendez, A. Arenillas, B. Fidalgo, Y. Fernandez, L. Zubizarreta, E.G. Calvo, J.M. Bermudez, Microwave heating processes involving carbon materials, Fuel Process. Technol. 91 (2010) 1–8.
[20] P. Kumar, K.H. Sandhage, The fabrication of near net-shaped spinel bodies by the oxidative transformation of Mg/Al_2O_3 precursors, J. Mater. Res. 13 (1998) 3423–3435.
[21] W. Yue, W. Zhou, Porous crystals of cubic metal oxides templated by cage-containing mesoporous silica, J. Mater. Chem. 17 (2007) 4947–4952.
[22] Z. Chen, E. Shi, W. Li, Y. Zheng, W. Zhong, Hydrothermal synthesis and optical property of nano-sized $CoAl_2O_4$ pigment, Mater. Lett. 55 (2002) 281–284.
[23] G. Jacobs, J.A. Chaney, P.M. Patterson, T.K. Das, J.C. Maillot, B.H. Davis, Fischer–Tropsch synthesis: study of the promotion of Pt on the reduction property of Co/Al_2O_3 catalysts by in-situ EXAFS of Co K and Pt LIII edges and XPS, J. Synchrotron Radiat. 11 (2004) 414–422.
[24] W. Chu, P.A. Chernavskii, L. Gengembre, G.A. Pankina, P. Fongarland, A.Y. Khodakov, Cobalt species in promoted cobalt alumina-supported Fischer–Tropsch catalysts, J. Catal. 252 (2007) 215–230.
[25] J. Sun, A.M. Karim, D. Mei, M. Engelhard, New insights into reaction mechanisms of ethanol steam reforming on $Co–ZrO_2$, Appl. Catal. B: Environ. 162 (2015) 141–148.
[26] M.P. Hyman, J.M. Vohs, Reaction of ethanol on oxidized and metallic cobalt surfaces, Surf. Sci. 605 (2011) 383–389.
[27] A.M. Karim, Y. Su, M.H. Engelhard, D.L. King, Y. Wang, Catalytic roles of Co^0 and Co^{2+} during steam reforming of ethanol on Co/MgO catalysts, ACS Catal. 1 (2011) 279–286.
[28] S.S.Y. Lin, D.H. Kim, M.H. Engelhard, S.Y. Ha, Water induced formation of cobalt oxides over supported cobalt/ceria–zirconia catalysts under ethanol-steam reforming reaction, J. Catal. 273 (2010) 229–235.